



HAL
open science

Size-dependent DNA mobility in cytoplasm and nucleus

Gergely L Lukacs, Peter Haggie, Olivier Seksek, Delphine Lechardeur, Neal Freedman, A. S. Verkman

► **To cite this version:**

Gergely L Lukacs, Peter Haggie, Olivier Seksek, Delphine Lechardeur, Neal Freedman, et al.. Size-dependent DNA mobility in cytoplasm and nucleus. *Journal of Biological Chemistry*, 2000, 275 (3), pp.1625-1269. 10.1074/jbc.275.3.1625 . hal-01604987

HAL Id: hal-01604987

<https://hal.science/hal-01604987>

Submitted on 1 Jun 2020

HAL is a multi-disciplinary open access archive for the deposit and dissemination of scientific research documents, whether they are published or not. The documents may come from teaching and research institutions in France or abroad, or from public or private research centers.

L'archive ouverte pluridisciplinaire **HAL**, est destinée au dépôt et à la diffusion de documents scientifiques de niveau recherche, publiés ou non, émanant des établissements d'enseignement et de recherche français ou étrangers, des laboratoires publics ou privés.

Copyright

Size-dependent DNA Mobility in Cytoplasm and Nucleus*

(Received for publication, August 3, 1999)

Gergely L. Lukacs^{‡§}, Peter Haggie, Olivier Seksek, D. Lechardeur[‡], Neal Freedman, and A. S. Verkman[¶]

From the Departments of Medicine and Physiology, Cardiovascular Research Institute, University of California, San Francisco, California 94143-0521 and [‡]Program in Cell and Lung Biology, Hospital for Sick Children, Department of Laboratory Medicine and Pathobiology, University of Toronto, Toronto, Ontario M5G 1X8, Canada

The diffusion of DNA in cytoplasm is thought to be an important determinant of the efficacy of gene delivery and antisense therapy. We have measured the translational diffusion of fluorescein-labeled double-stranded DNA fragments (in base pairs (bp): 21, 100, 250, 500, 1000, 2000, 3000, 6000) after microinjection into cytoplasm and nucleus of HeLa cells. Diffusion was measured by spot photobleaching using a focused argon laser spot (488 nm). In aqueous solutions, diffusion coefficients of the DNA fragments in water (D_w) decreased from 53×10^{-8} to 0.81×10^{-8} cm²/s for sizes of 21–6000 bp; D_w was related empirically to DNA size: $D_w = 4.9 \times 10^{-6}$ cm²/s [bp size]^{-0.72}. DNA diffusion coefficients in cytoplasm (D_{cyto}) were lower than D_w and depended strongly on DNA size. D_{cyto}/D_w decreased from 0.19 for a 100-bp DNA fragment to 0.06 for a 250-bp DNA fragment and was <0.01 for >2000 bp. Diffusion of microinjected fluorescein isothiocyanate (FITC) dextrans was faster than that of comparably sized DNA fragments of 250 bp and greater. In nucleus, all DNA fragments were nearly immobile, whereas FITC dextrans of molecular size up to 580 kDa were fully mobile. These results suggest that the highly restricted diffusion of DNA fragments in nucleoplasm results from extensive binding to immobile obstacles and that the decreased lateral mobility of DNAs >250 bp in cytoplasm is because of molecular crowding. The diffusion of DNA in cytoplasm may thus be an important rate-limiting barrier in gene delivery utilizing non-viral vectors.

The diffusional mobility of DNA fragments in cytoplasm is thought to be an important determinant of the efficacy of DNA delivery in gene therapy and antisense oligonucleotide therapy (1–3). Liposome-mediated gene transfer involves endocytic uptake, release from endosomes, dissociation of DNA from lipid, diffusion through cytoplasm, transport across nuclear pores, and diffusion to nuclear target sites (4–7). Although considerable attention has been given to the mechanisms of cellular DNA internalization, nuclear uptake, and subsequent molecular events, little is known about the diffusive properties of

introduced DNA fragments in cytoplasm and nucleus. It is not known whether the diffusion of DNA fragments is hindered by binding and steric interactions or how the size and physical structure of DNA affect its diffusional properties.

Recent studies have provided information about the diffusional mobilities of small and macromolecule-sized solutes in cytoplasm and nucleus. Spot photobleaching measurements indicated that small solutes diffuse freely and rapidly in cytoplasm and nucleus, with diffusion coefficients only 3–4 times lower than that in water (8, 9). Analysis of the individual factors slowing solute diffusion, including fluid-phase viscosity, binding, and collisional interactions, indicated that the principal barrier for diffusion of small solutes was collisional interactions due to macromolecular crowding (8). The “fluid-phase” viscosity of cytoplasm and nucleus, defined as the viscosity sensed by a small probe that does not interact with cellular components, was determined by time-resolved anisotropy (10) and ratio imaging of a viscosity-sensitive fluorescent probe (11) to be only 1.2–1.4 times greater than the viscosity of water. The translational diffusion of larger, macromolecule-sized solutes (FITC¹-labeled dextrans and Ficolls) in cytoplasm and nucleus was only 3–4-fold slower than in water for solutes <500–750 kDa (12) but was markedly slowed for larger solutes (11, 12). The diffusional mobilities of targeted green fluorescent protein chimeras have been measured recently in the aqueous phase of cytoplasm (13), mitochondria (14), and endoplasmic reticulum (15). Although these studies provide a starting point to predict the diffusional properties of DNA fragments, they do not account for the unique charge and structure of DNA that may strongly affect its interactions with cellular components and thus its diffusional mobility.

The purpose of this study was to measure the translational diffusion of DNA in cytoplasm and nucleus. Diffusion of microinjected fluorescein-labeled oligonucleotides and larger DNA fragments was measured by fluorescence recovery after photobleaching. It was found that the diffusion of small DNA fragments in cytoplasm was mildly impeded but became greatly hindered with increasing DNA size. The diffusion of DNA fragments of all sizes was severely restricted in the nucleus. These results have important implications regarding the barriers to DNA transit through cells.

MATERIALS AND METHODS

Labeled DNA Fragments—The 3000- and 6000-bp double-stranded DNA fragments were obtained by linearizing plasmids pBluescript SK and pGI2 (Promega), respectively. The 1000-bp DNA was obtained by digesting pBluescript with *Dra*I and *Eco*RI, generating fragments of 1200, 1000, and 700 bp. The 100-, 50-, and 2000-bp DNA fragments were generated by PCR amplification using human cystic fibrosis transmembrane conductance regulator (CFTR) cDNA as a template. The

* This work was supported by National Institutes of Health Grants DK43840, HL60288, DK35124, and HL59198, Gene Therapy Core Center Grant DK47766, Research Development Program Grant R613 from the National Cystic Fibrosis Foundation, a SPARXII award from the Canadian Cystic Fibrosis Foundation, and funds from the Lung Gene Therapy initiative of the Hospital for Sick Children. The costs of publication of this article were defrayed in part by the payment of page charges. This article must therefore be hereby marked “advertisement” in accordance with 18 U.S.C. Section 1734 solely to indicate this fact.

§ Scholar of Medical Research Council of Canada.

¶ To whom correspondence should be addressed: 1246 Health Sciences East Tower, Cardiovascular Research Inst., University of California, San Francisco, CA 94143-0521. Tel.: 415-476-8530; Fax: 415-665-3847; E-mail: verkman@itsa.ucsf.edu; http://www.ucsf.edu/verklab.

¹ The abbreviations used are: FITC, fluorescein isothiocyanate; PCR, polymerase chain reaction; bp, base pair(s).

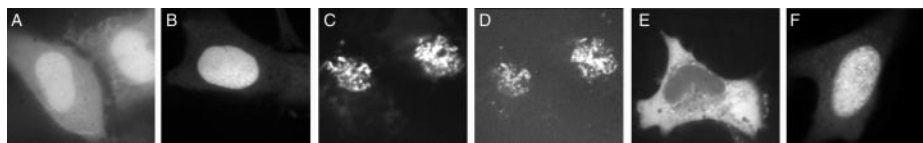


FIG. 1. Confocal fluorescence micrographs of HeLa cells after microinjection with fluorescein-labeled DNA fragments. Micrographs were taken with $\times 60$ oil immersion objective and cooled CCD camera as described under “Materials and Methods.” A and B, cytoplasm was microinjected with 21-mer double-stranded oligonucleotide. Micrographs were obtained at 2 min (A) and 5 min (B) after microinjection. C and D, cytoplasm injected with double-stranded linear 6000-bp DNA with micrographs recorded at 5 min (C) and 60 min (D) after microinjection. E and F, cytoplasm (E) and nucleus (F) microinjected with double-stranded 500-bp DNA fragment. Micrographs were obtained at 10 min after microinjection.

amplified DNAs corresponded to nucleotides 4357–4443, 300–800, and 200–2301, respectively, in the CFTR cDNA. The 250-bp DNA fragment was generated by PCR using yeast ubiquitin cDNA as template. DNAs were covalently labeled with fluorescein using the IT nucleic acid labeling kit (PanVera Corp.) according to the manufacturer’s instructions. The labeled DNA fragments were purified twice on Microspin columns and ethanol-precipitated. Fluorescein labeling did not alter DNA conformation as assessed by restriction enzyme and DNase I susceptibility (data not shown). The fluorescein-labeled 21-mer (5′-GGTTATCTAGACTCGAGCTC-3′) phosphorothioate oligonucleotide was synthesized by Research Genetics Inc., and the double-stranded 21-mer was obtained by annealing with its unlabeled complementary sequence. In some experiments, cells were microinjected with size-fractionated FITC dextrans (70, 580, and 2000 kDa) prepared as described previously (12).

Cell Culture and Microinjection—HeLa cells (ATCC CCL-2, passages 15–30) were cultured on 18-mm diameter round glass coverslips in DME H-21 medium supplemented with 5% fetal calf serum, penicillin (100 units/ml), and streptomycin (100 $\mu\text{g}/\text{ml}$). Cells were grown at 37 °C in 95% air, 5% CO_2 and used 1–2 days after plating at which time they were $\sim 80\%$ confluent. For microinjection, fluorescein-labeled DNAs were dissolved in calcium-free phosphate-buffered saline, and solutions were centrifuged ($10,000 \times g$, 10 min) to remove particulate matter. Microinjection was performed using an Eppendorf 5170 micromanipulator and 5242 microinjector. Glass needles were drawn from thin-walled filament capillaries (FHC, Brunswick, ME) with a vertical needle puller (Kopf, Tujunga, CA). Cells were microinjected with ~ 4 fl of solution at an injection pressure of 120 kilopascals over 0.5 s. Measurements were made at 23 °C at 5–45 min after microinjection unless otherwise specified.

Spot Photobleaching Measurements—An apparatus described previously (16) was modified to measure recovery curves over long times. The output of an argon ion laser (488 nm, Innova 70–4, Coherent Inc.) was modulated by a high contrast acousto-optic modulator (Brimrose Inc.) and directed onto the stage of an inverted epifluorescence microscope (Diaphot, Nikon). The excitation path also contained a fast shutter (open/close times < 2 ms), which was used to switch the probe beam on and off (beam on ~ 25 ms out of every 1–10 s) during data acquisitions over long times. The beam was reflected by a dichroic mirror (510 nm) onto the sample using an objective lens (Nikon $\times 20$ dry, numerical aperture 0.75; or Nikon $\times 60$ oil, numerical aperture 1.4). For most experiments, the laser beam power was set to 50–100 milliwatts (488 nm), and the attenuation ratio (the ratio of bleach to probe beam intensity) was set to 5000–10,000 to give $< 30\%$ bleach. Sample fluorescence was filtered by serial barrier (Schott glass OG 515) and interference (530 ± 15 nm) filters and detected by a gated photomultiplier. Signals were amplified and digitized at 1 MHz using a 14-bit analog-to-digital converter. Beam modulation, shutter state, photomultiplier gating, and data collection were software controlled. Signals were sampled prior to the bleach (generally 10^3 data points in 100 ms) and over three different time intervals after the bleach: high resolution data (1-MHz sampling rate) over 10–100 ms, low resolution data (generally 10^4 points) over 0.1–10 s, and long time data (generally 10^3 points averaged over 25 ms while shutter open, followed by specified delay).

For measurements in aqueous solutions, 2.5- μl solution volumes were “sandwiched” between two coverslips to produce aqueous layers of ~ 5 - μm thickness. Three to six individual recovery curves were generally averaged. For cell measurements, the coverglass containing the cultured cells (facing upward) was mounted in a perfusion chamber and positioned on the microscope stage. Measurements were made on different cells for analysis of individual recovery curves or groups of averaged recovery curves.

Photobleaching with Confocal Image Detection—A Nipkow wheel confocal microscope (Leitz upright microscope with Technical Instru-

ments K2-Bio coaxial-confocal attachment) and cooled CCD camera detector (Photometrics) were used to acquire cell images after bleaching. An electronically shuttered bleach beam from the argon laser was directed onto the cell sample from below using a Leitz $\times 25$ long working distance air objective. Cells were viewed from above by epifluorescence using the $\times 60$ oil immersion objective and fluorescein filter set. Software was written to coordinate the bleach pulse, excitation and camera shutters, and image acquisition.

Analysis of Photobleaching Data—Apparent D values were determined from $t_{1/2}$ using an experimentally determined calibration relation of $t_{1/2}$ versus D obtained with solutions of fluorescein in defined water/glycerol mixtures (8). $t_{1/2}$ values were determined from pre-bleach fluorescence and the fluorescence recovery time course as described previously (12). Data obtained in cells using the $\times 60$ objective were compared with the calibration relation obtained with the $\times 20$ objective using a correction factor of 9.3 determined from the ratio of $t_{1/2}$ measured using the $\times 20$ versus $\times 60$ objectives in cells expressing green fluorescent protein in their cytoplasm (13).

RESULTS

The diffusional mobilities of fluorescein-labeled DNAs were measured after microinjection into cytoplasm or nucleus of HeLa cells. Fig. 1 shows representative confocal micrographs of microinjected cells. After microinjection into cytoplasm, a double-stranded 21-mer phosphorothioate oligonucleotide accumulated rapidly in the nucleus (2- and 5-min micrographs shown in Fig. 1, A and B). Similar results were found for single-stranded phosphodiester and phosphorothioate oligonucleotides (not shown). In contrast, little diffusion away from the cytoplasmic microinjection site was found for a 6000-bp linear double-stranded DNA fragment at 5 min (Fig. 1C) and 60 min (Fig. 1D) after microinjection. (The nucleus is out of the image field in Fig. 1, C and D.) A 500-bp DNA fragment distributed through the cytoplasm (Fig. 1E) and nucleus (Fig. 1F) within a few minutes after microinjection but did not cross the nuclear membrane.

Spot photobleaching experiments were carried out for quantitative determination of diffusion coefficients. Fig. 2A shows photobleaching recovery curves for saline solutions of fluorescein-labeled DNA fragments. Measurements were carried out on thin solution layers between coverglasses using a $\times 20$ objective (spot diameter ~ 4 μm). The signals recovered to approximately the pre-bleach fluorescence as expected for unhindered probe diffusion in aqueous solutions. The recovery rates depended strongly on DNA size with $t_{1/2}$ increasing from 24 ms (oligonucleotide) to ~ 1500 ms (6000-bp DNA fragment). Fig. 2B shows a log-log plot of deduced diffusion coefficients (D_w) versus DNA molecular size (in kDa), with an empirical linear fit, $D_w = 4.9 \times 10^{-6} \text{ cm}^2/\text{s} \cdot [\text{bp size}]^{-0.72}$. For comparison D_w values for size-fractionated FITC dextrans are shown.

Spot photobleaching measurements were done in HeLa cells microinjected with the fluorescein-labeled DNA fragments. Cells were illuminated using a $\times 60$ oil immersion objective (spot diameter ~ 1.3 μm). As described under “Materials and Methods,” care was taken to avoid photobleaching by the probe beam, and bleach time and intensity were set to give bleach depth $< 30\%$ of initial intensity and bleach time under 5% of

FIG. 2. Spot photobleaching of fluorescein-labeled DNA fragments in saline solution. A, representative fluorescence recovery curves for indicated linear double-stranded DNA fragments in phosphate-buffered saline at 23 °C. Solution layer thickness was 5 μm , and the $\times 20$ objective lens was used. Bleach times were $< 2\%$ of recovery half-times, and bleach depth was maintained at 20–28%. B, diffusion coefficients (D_w , $\text{cm}^2/\text{s} \times 10^{-8}$) as a function of DNA size. D_w for FITC dextrans is shown for comparison.

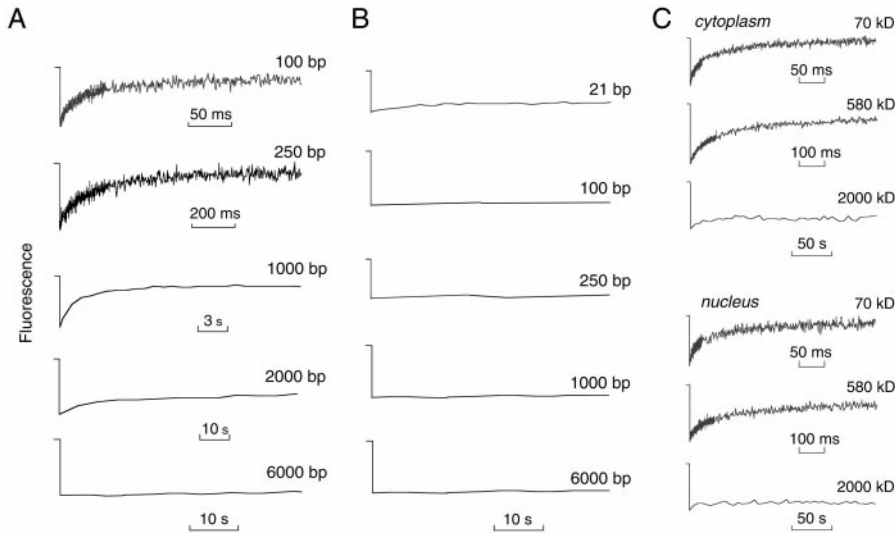
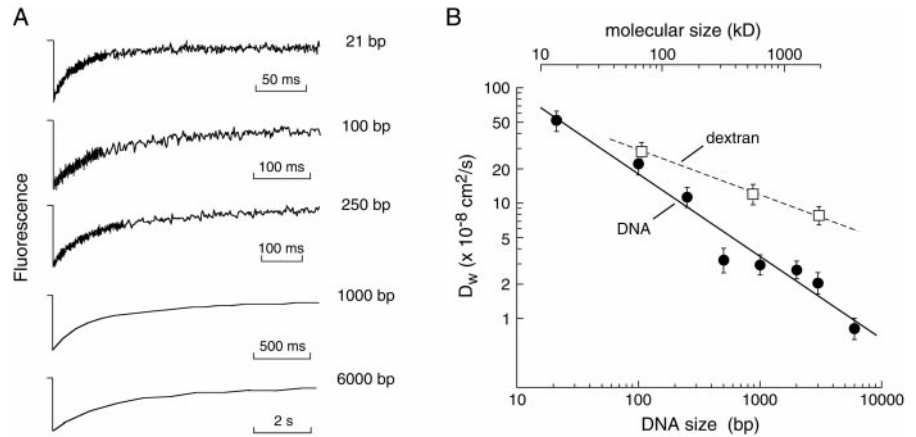


FIG. 3. Spot photobleaching measurements of fluorescein-labeled DNA and dextran diffusion in microinjected HeLa cells. Representative fluorescence recovery data ($\times 60$ oil immersion objective) in cytoplasm (A) and nucleus (B) of cells microinjected with indicated fluorescein-labeled DNA fragments at 23 °C. Data represent averaged recovery curves for three or more individual experiments. In each case bleach time was well under 5% of recovery $t_{1/2}$ and bleach depth was under 30%. C, fluorescence recovery curves for indicated microinjected FITC dextrans in cytoplasm and nucleus.

recovery half-time. Original recovery curves for the diffusion of fluorescein-labeled DNA fragments are shown in Fig. 3A for cytoplasm and Fig. 3B for nucleus. (Because the microinjected oligonucleotide disappeared very quickly from the cytoplasm, it was not possible to make an accurate photobleaching measurement of oligonucleotide diffusion in cytoplasm.) DNA diffusion in cytoplasm was strongly size-dependent. The majority of labeled DNA was mobile in cytoplasm for up to 1000 bp as shown by the nearly complete fluorescence recoveries. In contrast, DNAs of all sizes diffused very slowly in nucleus. Similar measurements were made in cytoplasm and nucleus microinjected with FITC dextrans in place of the fluorescein-labeled DNA fragments. Fig. 3C shows that the 70- and 580-kDa FITC dextrans diffused freely in cytoplasm and nucleus (equivalent to DNA sizes of 106 and 878 bp, respectively), whereas the 2000-kDa FITC dextran was essentially immobile.

Control studies were done to prove that the recovery signals above represented translational diffusion of the fluorescein-labeled DNA fragments. Measurements of fluorescence recovery rates were done as a function of spot diameter and bleach time/intensity (as done in Refs. 17 and 18). Recovery rates decreased with increasing bleach spot diameter, as expected for a diffusion-related process. Fig. 4A shows recovery curves for bleaching of the 250-bp DNA fragment using $\times 60$ and $\times 100$ objectives; the recovery $t_{1/2}$ increased by more than 2-fold for the lower power objective. The recovery rates were not dependent on solution O_2 content (Fig. 4A, lower curve), indicating that triplet state relaxation processes do not contribute to the fluorescence recovery. However, when samples containing fluorescein-labeled DNA fragments were bleached by a brief laser pulse, a very fast fluorescence recovery process (< 2 ms) was observed, as seen in Fig. 4B for the fluorescein-labeled oligonucleotide in nucleus. In contrast to the slower recovery processes in Fig. 3, the time course of the very fast process was not dependent on spot size ($t_{1/2}$ 1.7 ± 0.1 (S.E., $n = 7$) and 2.1 ± 0.3 ms for $\times 60$ and $\times 20$ objectives), was abolished in buffers saturated with 100% O_2 (Fig. 4B, lower curve), and was readily observed at low bleach intensities and short bleach times (not shown). As discussed in Refs. 17 and 19, this rapid reversible photophysical process probably arises from triplet state relaxation and is unrelated to DNA diffusion.

Fig. 4C shows serial fluorescence micrographs after bleaching a large spot in the cytoplasm or nucleus. Direct visualization is useful to identify any unusual compartmentation or other phenomena that might alter the interpretation of the quantitative spot photobleaching experiments in Fig. 3. In each case a pre-bleach micrograph is shown at the left; serial fluorescence micrographs at indicated times are shown at the right. Consistent with the spot photobleaching recovery curves, fluorescence recovery was seen for a 250-bp DNA fragment in cytoplasm over 10–25 s (top row of micrographs), whereas essentially no recovery was seen in nucleus (bottom row of micrographs). (The considerably slower recovery $t_{1/2}$ values in cytoplasm compared with data in Fig. 3A are because of the much larger spot size.) There was little compartmentation or major DNA-inaccessible compartments.

Fig. 5 summarizes relative DNA diffusion coefficients in cytoplasm (D_{cyto}) and nucleus (D_{nuc}) relative to that in water

(D_w). For comparison, D_{cyto}/D_w and D_{nuc}/D_w for microinjected FITC dextrans are shown (see "Discussion").

DISCUSSION

This study provides basic information about the diffusional mobility of naked DNA fragments in cytoplasm and nucleus. The DNA fragments were introduced by microinjection to study their mobilities in the aqueous compartments of cytoplasm and nucleus without complicating factors such as vesicular compartmentation and degradation resulting from prolonged incubation. After microinjection into the cytoplasm, small oligonucleotides diffused promptly into the nucleus where they became

remarkably hindered in their diffusion. A DNA fragment of 100 bp was fully mobile in cytoplasm with a diffusive rate only ~ 5 times slower than in water, similar to that of a comparably sized FITC dextran. The diffusion of larger DNA fragments in cytoplasm became remarkably slowed, with little or no diffusion for DNAs >2000 bp. In nucleus, DNA fragments of all sizes were nearly immobile on a distance scale of ~ 1 micron and a time scale of several minutes. In contrast, similar sized FITC dextrans up to 580 kDa diffused freely in the nucleus. The immobilization of DNA by the nucleus is probably because of extensive DNA binding to nuclear components, including the positively charged histones. These findings indicate that diffusion of DNAs can be a significant rate-limiting barrier in the cellular processing of plasmids and large DNA fragments, particularly when diffusion and nuclear uptake compete with degradation by cytosolic nucleases (20).

The microinjected oligonucleotide was rapidly taken up by the nucleus, such that little cytoplasmic fluorescence remained a few minutes after microinjection. This observation is consistent with the efficient accumulation of oligonucleotides in the nucleus that has been attributed to oligonucleotide binding to nuclear proteins (21) and active nuclear import (22). Our finding of impeded oligonucleotide mobility in nucleus is consistent with the avid nuclear accumulation of oligonucleotides. Politz *et al.* (23) recently reported the diffusion of fluorescein-labeled oligo(dA) and -(dT) (43-mers) in the nucleus of cultured rat myoblasts measured by fluorescence correlation spectroscopy. They found that although the majority of oligo(dT) was immobile, probably because of hybridization to poly(A) sequences, a significant fraction of the poly(dT) was free with an apparent diffusion coefficient of 4×10^{-7} cm²/s, nearly the same as that measured in aqueous solutions. From previous measurements (12) and data here showing that nuclear diffusion of non-reactive dextrans and Ficolls (0.5–500 kDa) is 3–5 times slower than in water, it is anticipated that nuclear diffusion of an oligonucleotide, even if it does not bind to nuclear components, must be substantially slower than in water. Further, rapid oligonucleotide diffusion appears to be inconsistent with the stable nuclear accumulation of oligonucleotides. The differences between the results here and those of Politz *et al.* (23) could be related to differences in the cells and/or oligonucleotides or possibly reversible photobleaching processes, which can be difficult to evaluate in fluorescence correlation spectroscopy measurements. We note that the recovery $t_{1/2}$ for the reversible recovery (Fig. 4B) would predict an apparent oligonucleotide diffusion coefficient of 1–2 times faster than that in water, which could be misinterpreted as rapid diffusion in

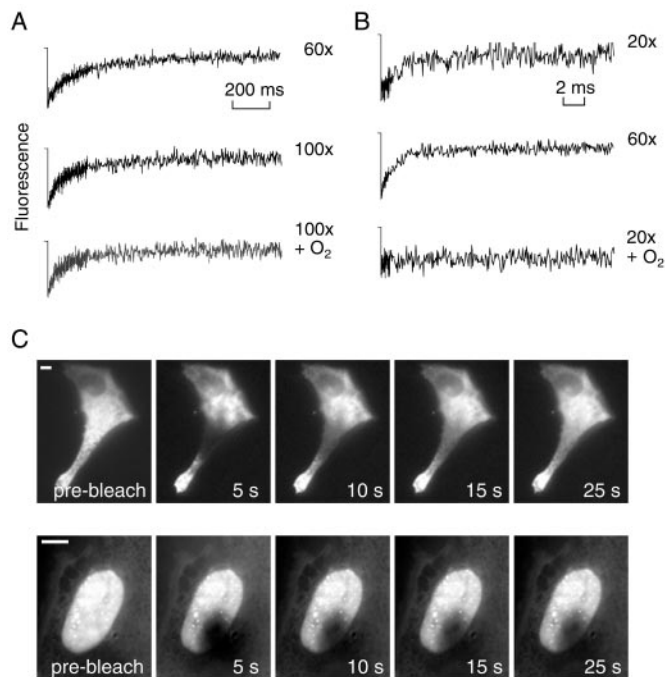


FIG. 4. Photobleaching of fluorescein-labeled DNA fragments. A, dependence of fluorescence recovery on spot size. Recovery curves are shown for 250-bp fluorescein-labeled DNA in cytoplasm measured using $\times 60$ and $\times 100$ objectives with bleach times of 4 ms. B, reversible photobleaching of fluorescein-labeled oligonucleotide in nucleus. Fast recovery of 21-bp fluorescein-labeled DNA was measured with 100- μ s bleach time with indicated objectives and in cells bathed in air versus 100 O₂-saturated solution (see text for explanation). C, serial fluorescence images were recorded at indicated times with $\times 60$ oil immersion objective. Pre-bleach images are shown at the left. Cytoplasm (top) and nucleus (bottom) were injected with a 250-bp fluorescein-labeled DNA fragment. Scale bar, 5 μ m.

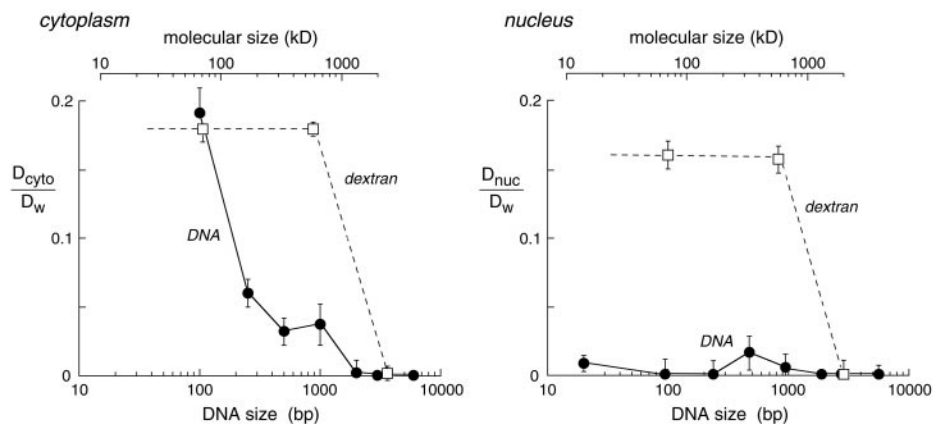


FIG. 5. DNA size dependence of relative diffusion coefficients in cytoplasm (D_{cyto}/D_w) and nucleus (D_{nuc}/D_w). Each point is the mean \pm S.E. for 5–15 independent measurements for DNA diffusion in cytoplasm (left) or nucleus (right). For comparison, D_{cyto}/D_w and D_{nuc}/D_w values for microinjected FITC dextrans (open squares) are as shown.

nucleus. The imaging study in Fig. 4C confirms the relative immobility of the oligonucleotide in nucleus.

The DNA diffusion coefficients measured here in solution are in general agreement with the few reported data. Bjorling *et al.* (24) used fluorescence correlation spectroscopy to detect DNA products formed during PCR. They reported that the relative translational diffusion coefficient decreased linearly with the length of double-stranded DNA fragments, decreasing 5-fold with fragments of 50–500 nucleotides. Fishman and Patterson (25) estimated the diffusion coefficient of a linearized 3.7-kilobase plasmid by low angle dynamic light scattering to be 2.9×10^{-8} cm²/s. We found that the DNA diffusion coefficient decreased by 65-fold with increasing DNA size from 21 to 6000 bp. This decrease is quite different from that predicted for a spherical molecule, indicating the complex hydrodynamic properties of DNA with respect to translational diffusion.

There was a dramatic reduction of DNA diffusive rates in cytoplasm as DNA size increased beyond 1000 bp (660 kDa). Whereas the relative diffusion coefficient of DNA in cytoplasm compared with water (D_{cyto}/D_w) was approximately unity for small oligonucleotides, D_{cyto}/D_w progressively decreased to 0.19, 0.067, and 0.032 for DNA fragments of 100, 250, and 500 bp, respectively. The diffusion of DNAs of 3000 bp or greater was immeasurably slow. The slowing of DNA diffusion could represent a combination of binding and crowding effects. We believe that binding effects are not primarily responsible for the slowed diffusion of large DNA fragments because binding interactions should not depend strongly on DNA size. Thus molecular crowding and collisional interactions probably are responsible for the slowed DNA diffusion. Yarmola *et al.* (26) measured DNA diffusion in a 1% agarose gel from band spreading in the absence of an electric field. The DNA diffusion coefficient decreased from 1.7 to 0.2×10^{-8} cm²/s for DNA size of 1–3 kilobases. The substantially more crowded cellular environment, in which 10–15% of cytoplasm is occupied by macromolecules (8), is expected to produce an even stronger dependence of intracellular diffusion on DNA size.

The very slow diffusion of plasmid-size DNA fragments in cells is an important observation with regard to gene therapy. Vectors and cellular factors that enhance cytoplasmic DNA mobility may thus have value in increasing the efficacy of gene expression. The slow diffusion of plasmid DNA in the cytosol

has probably necessitated the evolution of efficient packaging and transport mechanisms to transport viral DNA across the cytoplasm. Interactions between viral capsid proteins and the microtubular network and/or the actin cytoskeleton appears to account for the efficient nuclear targeting of viral particles (27). The vectorial transport of viruses to the nucleus could thus serve as a paradigm to design more efficient DNA delivery systems to improve non-viral gene delivery methods.

REFERENCES

1. Hope, M. J., Mul, B., Ansell, S., and Ahkong, Q. (1998) *Mol. Membr. Biol.* **15**, 1–14
2. Kashiwara, N., Maeshima, Y., and Makino, H. (1998) *Exp. Nephrol.* **6**, 84–88
3. Ho, P. T., and Parkinson, D. R. (1997) *Semin. Oncol.* **24**, 187–202
4. Xu, Y., and Szoka, F. C. (1996) *Biochemistry* **35**, 5616–5623
5. Friend, D. S., Papahadjopoulos, D., and Debs, R. J. (1996) *Biochim. Biophys. Acta* **1278**, 41–50
6. Wrobel, I., and Collins, D. (1995) *Biochim. Biophys. Acta* **1235**, 296–304
7. Zabner, J., Fasbender, A., Moninger, T., Poellinger, K. A., and Welsh, M. J. (1995) *J. Biol. Chem.* **270**, 18997–19007
8. Kao, H. P., Abney, J. R., and Verkman, A. S. (1993) *J. Cell Biol.* **120**, 175–184
9. Bicknese, S., Periasamy, N., Shohet, S. B., and Verkman, A. S. (1993) *Biophys. J.* **165**, 1272–1282
10. Fushimi, K., and Verkman, A. S. (1991) *J. Cell Biol.* **112**, 719–725
11. Luby-Phelps, K., Mujundar, S., Mujundar, R., Ernst, L., Galbraith, W., and Waggoner, S. (1993) *Biophys. J.* **65**, 236–242
12. Seksek, O., Biwersi, J., and Verkman, A. S. (1997) *J. Cell Biol.* **138**, 131–142
13. Swaminathan, R., Hoang, C. P., and Verkman, A. S. (1997) *Biophys. J.* **72**, 1900–1907
14. Partikian, A., Olveczky, B., Swaminathan, R., Li, Y., and Verkman, A. S. (1998) *J. Cell Biol.* **140**, 821–829
15. Dayel, M. J., Hom, E. F., and Verkman, A. S. (1999) *Biophys. J.* **76**, 2843–2851
16. Kao, H. P., and Verkman, A. S. (1996) *Biophys. Chem.* **59**, 203–210
17. Periasamy, N., Bicknese, S., and Verkman, A. S. (1996) *Photochem. Photobiol.* **63**, 265–271
18. Swaminathan, R., Bicknese, S., Periasamy, N., and Verkman, A. S. (1996) *Biophys. J.* **71**, 1140–1151
19. Song, L., Varma, C. A., Verhoeven, J. W., and Tanke, H. J. (1996) *Biophys. J.* **70**, 2959–2968
20. Lechardeur, D., Sohn, K. J., Haard, M., Joshi, P. B., Monck, M., Graham, R. W., Beatty, B., Squire, J., O'Brodovich, H., and Lukacs, G. L. (1999) *Gene Ther.* **6**, 482–497
21. Leonetti, J. P., Mechti, N., Degols, G., Gagnor, C., and Lebleu, B. (1991) *Proc. Natl. Acad. Sci. U. S. A.* **88**, 2702–2706
22. Zelphati, O., and Szoka, F. C. (1996) *Pharm. Res. (N. Y.)* **13**, 1367–1372
23. Politz, J. C., Browne, E. S., Wolf, D. E., and Pederson, T. (1998) *Proc. Natl. Acad. Sci. U. S. A.* **95**, 6043–6048
24. Bjorling, S., Kinjo, M., Folders-Papp, Z., Hagman, E., Thybert, P., and Rigler, R. (1998) *Biochemistry* **37**, 12971–12978
25. Fishman, D. M., and Patterson, G. D. (1996) *Biopolymers* **38**, 535–552
26. Yarmola, E., Sokoloff, H., and Chrambach, A. (1996) *Electrophoresis* **17**, 1416–1419
27. Sodeik, B., Ebersold, M. W., and Helenius, A. (1997) *J. Cell Biol.* **136**, 1007–1021

Size-dependent DNA Mobility in Cytoplasm and Nucleus

Gergely L. Lukacs, Peter Haggie, Olivier Seksek, D. Lechardeur, Neal Freedman and A. S. Verkman

J. Biol. Chem. 2000, 275:1625-1629.

doi: 10.1074/jbc.275.3.1625

Access the most updated version of this article at <http://www.jbc.org/content/275/3/1625>

Alerts:

- [When this article is cited](#)
- [When a correction for this article is posted](#)

[Click here](#) to choose from all of JBC's e-mail alerts

This article cites 27 references, 8 of which can be accessed free at <http://www.jbc.org/content/275/3/1625.full.html#ref-list-1>